Clays and Clay Minerals, Vol. 42, No. 6, 679–688, 1994.

DEVELOPMENT OF MICROPOROSITY IN CLINOCHLORE UPON HEATING

F. VILLIERAS,[1] J. YVON,[1] J. M. CASES,[1] P. DE DONATO,[1] F. LHOTE,[2] AND R. BAEZA[3]

[1] Laboratoire Environnement et Minéralurgie, UA 235 du CNRS, rue du Doyen Marcel Roubault, BP 40, 54 501 Vandoeuvre les Nancy cedex, France

[2] Centre de Recherches Pétrographiques et Géochimiques, CNRS, 15 rue Notre Dame des Pauvres BP 20, 54 501 Vandoeuvre les Nancy cedex, France

[3] Talc de Luzenac, BP 1162, 31 036 Toulouse cedex, France

Abstract—The "modified chlorite structure" forms by the dehydroxylation of the interlayer octahedral sheet of magnesian chlorite at around 500°C and results in a structure with a basal spacing near 27 Å (Brindley and Chang 1974). This process involves drastic textural modifications as indicated by gas adsorption experiments which reveal the formation of structural micropores. Infrared spectroscopy as well as thermogravimetry and mass spectrometric analysis show that these micropores are filled with molecular atmospheric water, carbon dioxide, nitrogen, argon and hydrocarbons which condense once the samples cool down. A high temperature treatment is needed in order to release the different phases. A heterogeneous dehydroxylation mechanism is proposed in which micropores are formed in donor regions and magnesium and oxygen are concentrated in acceptor regions. This leads to a 27 Å structure with micropore zones and enriched interlayer oxide zones alternating along the z-axis of the mineral.

Key Words—Clinochlore, Dehydroxylation, Micropores.

INTRODUCTION

Among trioctahedral layer silicates, chlorites show particularly interesting thermal reactions due to the presence of two distinct hydrous octahedral sheets (Brindley and Lemaitre 1987). Thus, their thermal transformation occurs in two steps: 1) dehydroxylation of the hydroxyl groups of the interlayer octahedral sheet around 550°C and 2) dehydroxylation of the 2:1 layer around 800°C. The second reaction is immediately followed by recrystallization of high temperature species. In the case of magnesian chlorites, these high temperature phases are Mg-spinel, forsterite and enstatite. The dehydroxylation temperature is a function of particle size (Sabatier 1950) and octahedral composition (Caillère and Hénin 1960). Weiss and Rowland (1956) showed that the dehydroxylation of the brucite-like sheet of clinochlore is accompanied by an increase in intensity of the (001) basal reflection and a loss in intensity of the (002) and (003) reflections. Concomitantly, the remaining reflections ((001), (004) and (005)) are shifted towards smaller spacings. Brindley and Ali (1950) studied the thermal modifications of powders and flakes of Mg-chlorites heated to different temperatures and observed modifications of the basal reflections that confirmed Weiss's observations. They also showed that, after dehydroxylation of the interlayer sheet, about two-thirds of the octahedral cations have moved from the central plane in the octahedral sheet to sites previously occupied by hydroxyls. Brindley and Chang (1974) observed long basal spacings of about 27 Å after dehydroxylation, which they interpreted as the result of short range migration of cations of the interlayers into two alternate oxide layers. Differences in the electrostatic interactions of interlayers with the 2:1 layers were invoked to explain this arrangement. The modifications observed when chlorites are heated under atmospheric pressure occur in the same way when hydroxide layer dehydroxylation is performed under high pressure (Bai *et al* 1993). The same authors have shown that back reaction can occur when experiments are carried out at pressures over 500 bars.

Spectroscopic methods, such as infrared spectroscopy, were not used to study the thermal modifications of chlorites, although infrared spectroscopy examines the environment of adsorbed water, hydroxyl, and cations. Furthermore, infrared spectroscopy is very sensitive to short range disorder (Farmer 1974a; Bachiorrini and Murat 1986; Delmastro *et al* 1989) i.e., infrared studies of the thermal transformation of dioctahedral phyllosilicates have revealed the presence of pentacoordinated aluminum (Heller *et al* 1962; Farmer 1974b; Delmastro *et al* 1989).

Infrared spectra of Mg-chlorites generally exhibit three OH stretching bands at 3680, 3570 and 3420 cm^{-1}. The first one is assigned to hydroxyls of the 2:1 layer and the other two, to hydroxyls of the interlayer sheet which are hydrogen bonded to oxygens of the tetrahedral sheet (Shirozu 1980, 1985). In the 1100–400 cm^{-1} region the IR spectra can be divided into three frequency domains:

1) in the 1000 cm^{-1} range absorption peaks are assigned to lattice vibrations;
2) in the 850–650 cm^{-1} range, the vibrations at 827, 750 and 670 cm^{-1} are assigned to tetrahedral Al-O

Table 1. Chemical composition of chlorites P and M.

	Chlorite P (weight %)	Chlorite M (weight %)
SiO_2	31.22	35.89
Al_2O_3	18.93	16.33
Fe_2O_3	1.72	2.20
MgO	33.15	32.90
CaO	1.18	0.30
TiO_2	traces	0.80
P_2O_5	0.78	0.30
P.F.	12.31	11.41
Total	99.29	100.13

Table 2. Mineralogical composition of chlorites P and M.

	Chlorite P (weight %)	Chlorite M (weight %)
Chlorite	94.8 ± 1	80.3 ± 1
Talc	1.7 ± 1	17.7 ± 1
Quartz	0.9 ± 1	0
Dolomite	0.2 ± 0.5	0.1 ± 0.5
Apatite	1.5 ± 0.5	0.6 ± 0.5
Anatase		0.8 ± 0.5
Zircon		traces
Graphite		traces
Total	98.3	99.1

vibrations (Farmer 1974c), interlayer (SiAl)O–OH libration (Shirozu and Ishide 1982) and a combination of OH libration and two lattice vibrations (Shirozu and Ishide 1982) respectively;

3) in the 450–470 cm^{-1} region peaks are assigned to lattice vibrations and OH translational vibrations (Farmer 1974c).

This paper reports on structural and textural changes that occur when the interlayer octahedral sheet of Mg-chlorites dehydroxylates. By using a wide range of experimental techniques (thermogravimetry, X-ray diffraction, infrared spectroscopy, gas adsorption and mass spectrometric analysis), a new mechanism of thermal decomposition of the interlayer octahedral sheet is proposed.

EXPERIMENTAL

Materials

Two different clinochlores were used in this study. Both are from the ore body of Trimouns (Pyrénées, France) and were provided by Talc de Luzenac S.A. The first one, referred to as chlorite M, formed from the alteration of a mica schist, whereas the second one, referred to as chlorite P, formed during the hydrothermal transformation of a pegmatite. The chemical and mineralogical compositions of these samples are presented in Tables 1 and 2. Chlorite M contains about 20% talc and a few percent of various accessory minerals such as dolomite, apatite, zircon, titanite, graphite. Chlorite P is nearly talc free (2%) and contains apatite (2%) and some carbonates, apatite and quartz.

Both chlorites are microcrystalline aggregates of crystallites smaller than 10 μm (De Parseval 1992; Villiéras 1993) and were dry ground to similar sizes. Particle size distributions were determined using a Laser diffractometer (Mastersizer, Malvern Instruments). The D_{50} values are 28 and 14 μm for clinochlores M and P, respectively.

Thermal analysis

An Ugine-Eyraud B70 balance (Setaram) with a universal TG-TD head was used for combined thermogravimetric and thermodifferential analyses. Two hundred mg of sample were heated in a platinum crucible from room temperature to 1030°C using a 2°C/minute heating rate. Temperature, sample weight, and differential temperature were recorded simultaneously on a PC computer.

Isothermal pyrolysis

Calcinations were carried out, in air, in a muffle furnace (Prolabo) equilibrated at the desired temperature before introducing the sample. Fifteen g and 30 g of cold P and M sample powders, respectively, were placed in the hot furnace using a rectangular silica holder. Heating times varied between five minutes and two hours and temperatures varied between 400 and 1100°C.

X-ray diffraction

X-ray powder diffraction patterns were obtained on a Jobin-Yvon SIGMA 2080 reflecting diffractometer using Cu $K_{\alpha 1}$ radiation. Patterns were recorded on quenched samples at a scan rate of 2 degrees per minute.

Infrared spectroscopy

Infrared spectra were recorded on a Fourier transform infrared spectrometer (model IFS 88, Bruker). Three different types of IR techniques were used: 1) conventional transmission spectroscopy of pressed KBr pellets (2 mg of sample diluted in 148 mg of KBr) 2) transmission microspectroscopy of 20 μm diameter selected areas of the same KBr pellets and 3) diffuse reflectance spectroscopy of powders (70 mg sample diluted in 370 mg of KBr). The diffuse part of the spectra was collected with a Harrick accessory. This last technique enhances the bands of weak intensities and, in particular, the absorption bands corresponding to surface species (Griffiths and Haseth 1986). Before use, KBr was stored at 100°C to remove H_2O.

Argon adsorption

Argon surface areas were measured with a home-built apparatus based on a continuous volumetric procedure (Michot *et al* 1990). Surface areas were calculated according to the BET equation (Emmet and Brunauer 1937),

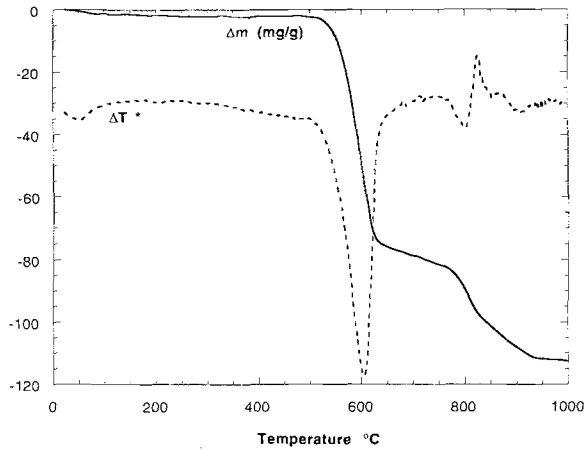

Figure 1. Thermogravimetric (Δm) and thermodifferential (ΔT) analysis of chlorite M. *: arbitrary unit.

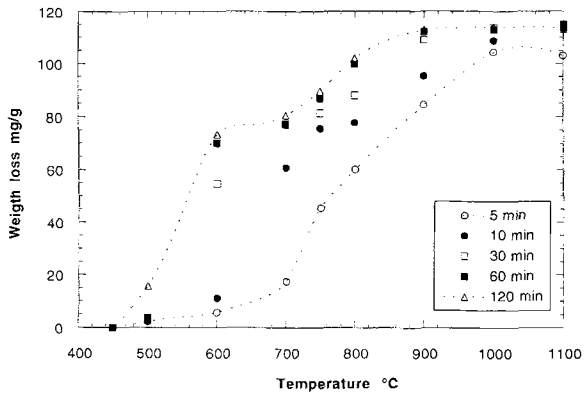

Figure 2. Weight loss of chlorite M versus temperature; influence of heating time.

assuming a value of 13.8 Å^2 for the cross sectional area of argon (McClellan and Harnsberger 1967).

Mass spectrometric analysis

Mass spectrometric analyses were done at the Centre de Recherches Pétrographiques et Géochimiques using the procedure described by Zimmermann *et al* (1988). The gases are extracted under vacuum and separated using cold traps, oxidation and reduction furnaces. Detection limits are 0.5 to 1 × 10^{-7} mol for H_2O, 3 × 10^{-8} mol for CO_2, and about 2 × 10^{-8} mol for H_2, N_2, CO, CH_4 and Ar.

RESULTS

Thermal analysis

Thermogravimetric and thermodifferential curves (Figure 1) are typical of powdered clinochlores. The DTA curves exhibit two endothermic peaks and one sharp exothermic peak. The release of H_2O from the interlayer octahedral sheet produces the first endothermic peak, around 600°C. Water from the 2:1 layer, released around 800°C, produces the second endothermic peak, immediately followed by the exothermic peak, around 830°C corresponding to recrystallization to spinel, forsterite and enstatite. The temperature of the peaks are similar for the two samples (Table 3). In the case of chlorite M, a weight loss around 900°C corresponds to talc dehydroxylation.

Chlorite M was heated in air at constant temperatures at intervals of 100°C from 400 to 1100°C. Heating times at each temperature were 5, 10, 30, 60 and 120 minutes. The weight loss was determined for each sample after cooling (Figure 2). After 5 minutes heating, the samples were found to be heterogeneous as the surface reacted more rapidly than the interior. This static method leads to lower reaction temperatures than the TGA method: dehydroxylation of the interlayer and 2:1 layers start between 400 and 500°C and, 700 and 800°C, respectively. Equilibrium is reached in 60 minutes, except for the 500°C experiment. Therefore, experiments were standardized on samples heated from 400 to 750°C at each 50°C for two hours.

X-ray diffraction (XRD)

Modifications in the X-ray diffraction patterns due to heating (Figure 3) are similar for the two samples and to the observations of Brindley and Chang (1974) and Weiss and Rowland (1956). The first structural transformations occur between 450 and 500°C. The intensity of the (001) reflection increases, the (002) reflection disappears, the intensity of the (003) and (004) reflections decrease and the (005) reflection re-

Table 3. Weight loss and peak temperatures obtained by thermal analysis.

	Hydroxide layer	2:1 layer	Other minerals
Pegmatitc chlorite			
Weight loss (mg/g)	87 ± 1	29 ± 1	7 ± 2 (Dolomite)
T endo. (°C)	597 ± 2	803 ± 2	
T exo. (°C)		829 ± 2	
Micaschist chlorite			
Weight loss (mg/g)	76 ± 1	26 ± 1	
T endo. (°C)	595 ± 2	800 ± 2	8 ± 1 (Talc)
T exo. (°C)		824 ± 2	

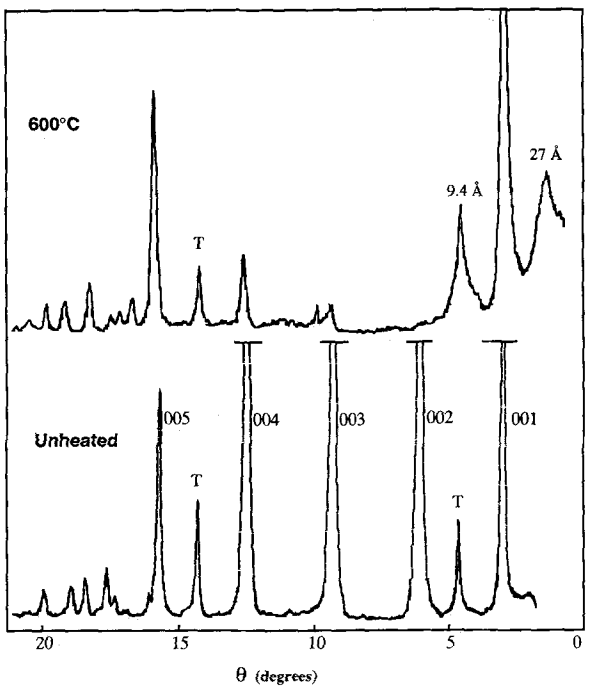

Figure 3. X-ray diffraction patterns recorded at room temperature of unheated chlorite P and chlorite P heated at 600°C for 2 hours. The intensity of the 005 reflection corresponds approximately to 30% of the most intense peaks (004 in the case of pattern a and 001 in the case of pattern b). T: talc.

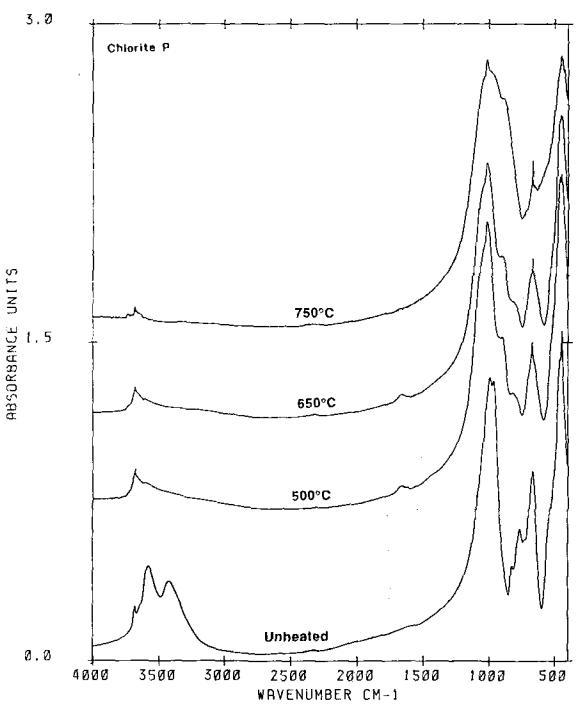

Figure 4. Transmission infrared spectra of unheated and heated chlorite P.

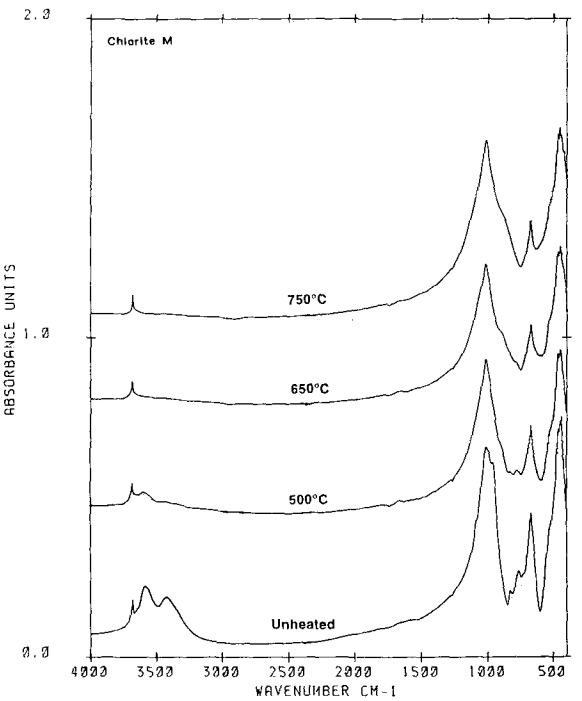

Figure 5. Transmission infrared spectra of unheated and heated chlorite M.

mains strong. New reflections appear at 26–27 Å (broad band) and 9.4 Å. These changes are completed at 550°C and the patterns do not exhibit any significant changes up to 750°C. At 750°C, the structure collapses and recrystallization to forsterite, enstatite and spinel occurs between 800 and 1000°C.

Infrared spectroscopy

The evolution of the IR spectra with heating was observed in both transmission (Figures 5 and 6) and diffuse reflectance (Figures 7 and 8) modes.

4000–1500 cm^{-1} range. Changes in the IR spectra appear at 500°C (Figures 4 to 7). In the case of chlorite P, the 3580 and 3428 cm^{-1} stretching bands of the brucitic hydroxyls disappear. In the case of chlorite M, these bands decrease and shift to 3593 and 3447 cm^{-1} (Figures 5 and 7). Infrared microscopy experiments show that, for chlorite M, at this temperature, interlayer hydroxyls of small particles and of the surface of large particles have reacted whereas the core of large particles still contains unreacted hydroxyl groups (Figure 8). At this stage, molecular water can be observed in the two samples (two bending modes at 1660 and 1610 cm^{-1}), particularly noticeable in the diffuse reflectance spectra (Figures 6 and 7). This water is still present in samples heated to 700°C (Figures 7 and 8) and disappears at 750°C (Figures 6 and 7), together with a part of the stretching vibration of the 2:1 hydroxyls at 3670 cm^{-1}. Bands between 2200 and 1700

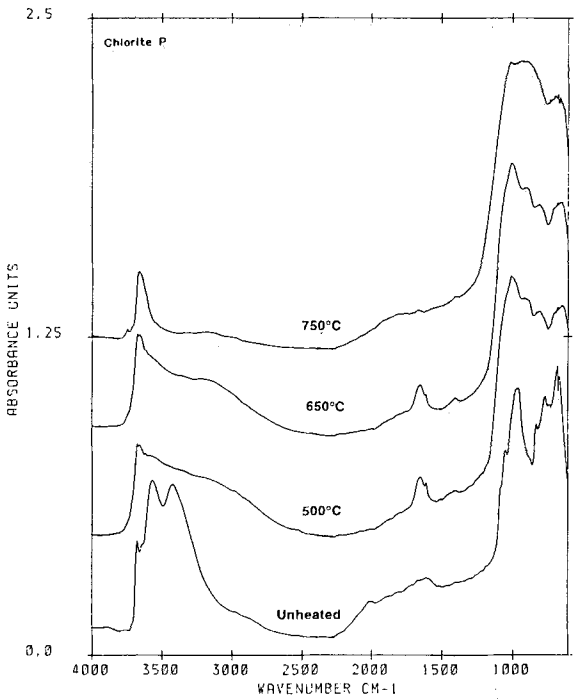

Figure 6. Diffuse reflectance infrared spectra of unheated and heated chlorite P.

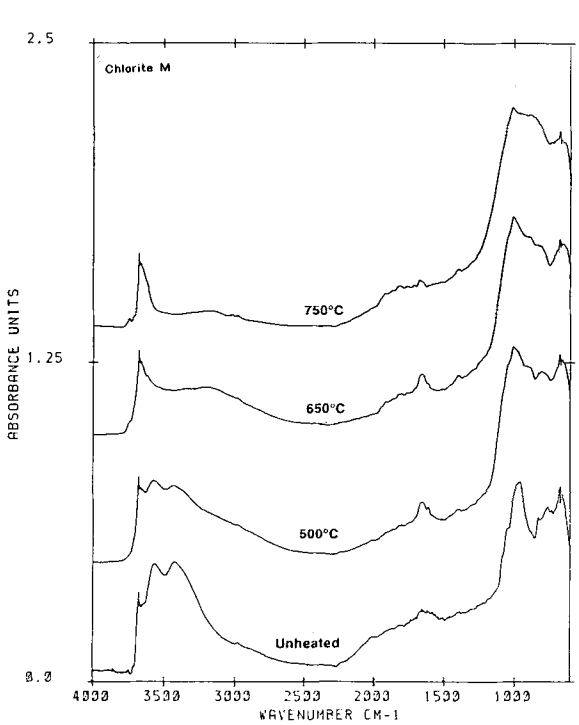

Figure 7. Diffuse reflectance infrared spectra of unheated and heated chlorite M.

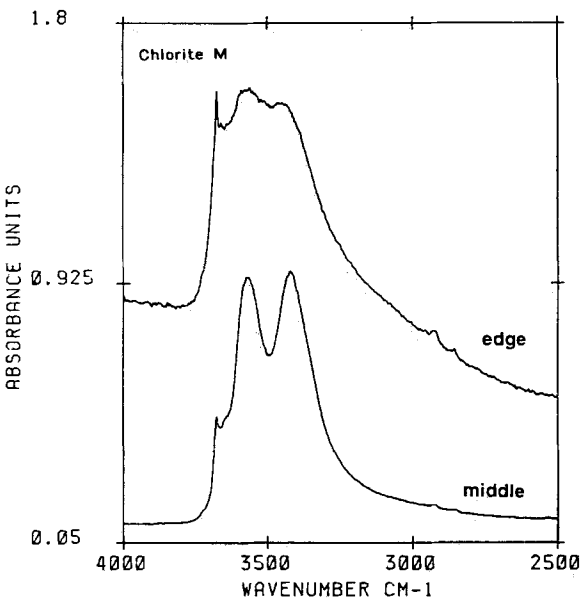

Figure 8. Transmission microspectroscopy spectra of chlorite M heated at 500°C obtained at the edge and in the middle of one single large particle.

cm^{-1} correspond to harmonic combination of bands between 400 and 1000 cm^{-1}.

1500–400 cm^{-1} range. Dehydroxylation of the OH groups of the interlayer octahedral sheet changes the Si-O stretching bands in the 1100–900 cm^{-1} range into one single broad band which broadens between 500 and 750°C (Figures 4 and 5). This could indicate short range disordering in the tetrahedral sheet of the 2:1 layer (Bachiorrini and Murat 1986; Delmastro *et al* 1989). This disorganization is further indicated by shoulders near 900 and 800 cm^{-1} which could be assigned to the modification of the tetrahedral Al-O environment as the 827 cm^{-1} vibration disappears after dehydroxylation. As expected, the (SiAl)O–OH interlayer libration at 750 cm^{-1} disappears. The 670 cm^{-1} decreases and the 450–470 cm^{-1} group is not affected.

Specific surface areas

Argon adsorption isotherms (Figure 9) were performed on four samples (Table 4). The unheated chlorite, the chlorite calcined at 750°C and the chlorite calcined at 600°C and outgassed at 100°C have similar BET specific surface area: 2.3, 2.2 and 1.4 $m^2 \cdot g^{-1}$, respectively. The shape of the isotherm obtained on the chlorite calcined at 600°C and outgassed at 480°C is typical of a microporous solid (Type I in the classification of Brunauer *et al* 1940). Its "equivalent" specific surface area is 26.4 $m^2 \cdot g^{-1}$.

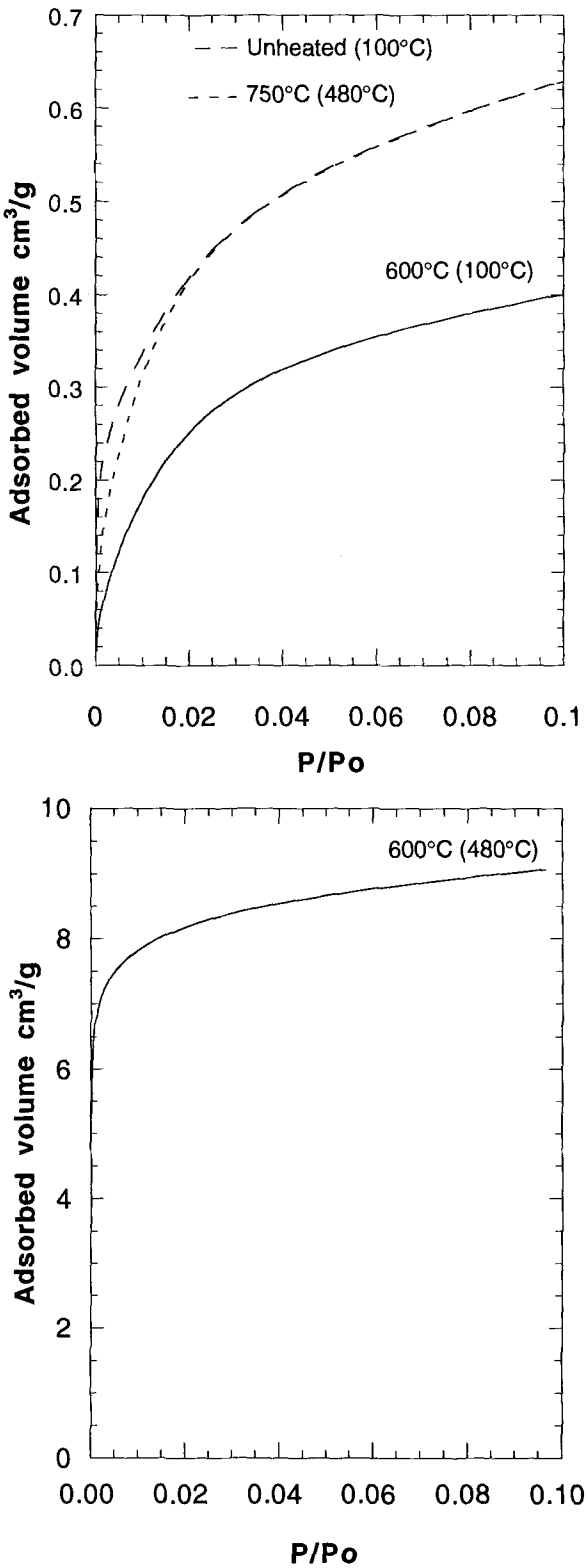

Figure 9. Argon adsorption isotherms at 77 K on chlorite M heated and outgassed in various conditions. The first value corresponds to the heating temperature, the value in brackets indicates the outgassing temperature.

Table 4. Argon specific surface area of chlorite M calcined and outgassed at different temperatures.

Calcination temperature (°C)	Outgassing temperature (°C)	Specific surface area (m^2/g)
Uncalcined	100	2.3
600	100	1.4
600	480	26.4
750	480	2.2

Mass spectrometric analyses

Mass spectrometric analyses were done to obtain information about the nature of the materials filling the micropores. The sample M calcined at 550°C was heated under vacuum at 200, 400 and 500°C. Numerous gases, H_2O, CO_2, N_2, Ar and H_2, were detected. H_2 originates from the reduction of H_2O (Escoubes and Karchoub 1977). Some masses corresponding to the splitting of organic compounds were also observed. The quantities of gases obtained for each temperature are reported in Table 5.

DISCUSSION

XRD, FTIR and TGA, show that the first modifications of chlorite occur between 450 and 500°C. These modifications affect the interlayer of the mineral as confirmed by the IR spectra (OH stretching). Reaction starts at the perimeter of the particles and proceeds towards the center as evidenced by infrared microscopy experiments. The modified chlorite exists from 550°C to 700°C. The 14 Å spacing of the original mineral is conserved but a long basal spacing develops at 26–27 Å with its third reflection at 9.4 Å. The peaks corresponding to these reflections are rather broad.

FTIR spectra indicate that molecular water is trapped in the dehydroxylated particles. In addition, thermogravimetric analyses carried out on chlorites calcined between 500 and 700°C reveal a weight loss between 450 and 520°C (Figure 10 and Table 6). This weight loss changes with the calcination temperature, with a maximum value for samples heated between 500°C and 550°C. It then decreases in samples calcined at 600°C to 700°C and disappears in those calcined at 750°C. To show that this weight loss corresponds to

Table 5. Mass spectrometric analysis of chlorite M heated at 550°C.

	25°–200°C	200°–400°C
H_2O (mg/g, ±0.05)	0.32	8.40
H_2 (mg/g, $\pm 1 \times 10^{-7}$)	0	1.1×10^{-6}
CO_2 (mg/g, ±0.005)	2.1×10^{-2}	1.3×10^{-1}
N_2 (mg/g, ±0.005)	1.7×10^{-3}	3.2×10^{-2}
Ar (mg/g, ±0.0004)	0	6.4×10^{-4}
Total (mg/g, ±0.060)	0.34	8.56

Table 6. Weight loss measured between 480° and 520°C on chlorites calcined between 500° and 750°C.

Calcination temperature (°C)	P chlorite (mg/g)	M chlorite (mg/g)
500	12.4	8.1
550	12.9	9.0
600	10.3	7.3
650	7.8	6.7
700	10.1	4.8
750	1.3	3.0

the trapped molecular water observed in the IR spectra, the relative water content (*RWC*) of the dehydroxylated chlorites was evaluated from the IR transmission measurements using the formula:

$$RWC = \frac{\text{area between 1775 and 1500 cm}^{-1}}{\text{area between 1150 and 720 cm}^{-1}} \times K$$

where K is a normalization factor which represents the extra weight loss obtained by thermogravimetric analysis between 450 and 520°C for the chlorite calcined at 550°C.

The Si-O-Si band at 1000 cm^{-1} was used as a reference, because it is nearly unaltered in samples heated between 500 and 700°C. Figure 11 presents the plot of *RWC* and of the weight loss measured by TGA versus calcination temperature. The correlation between TGA and FTIR estimations is good. Therefore, the weight loss observed by TGA between 450 and 520°C can be assigned to water trapped in micropores. Such an outgassing temperature is surprisingly high for water adsorbed in micropores. Indications can be obtained from the FTIR spectra. Indeed, the 1660 cm^{-1} band is accompanied by a small shoulder at 1610 cm^{-1}. This pattern is typical of microporous modulated clay minerals such as sepiolite or palygorskite (Hayashi *et al* 1969). The 1660 cm^{-1} band can be assigned to zeolitic

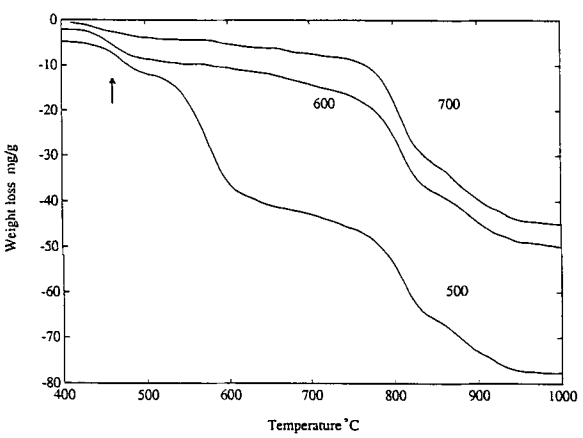

Figure 10. Thermogravimetric analyses of chlorite M previously heated. The extra weight loss between 480 and 520°C is noted by an arrow.

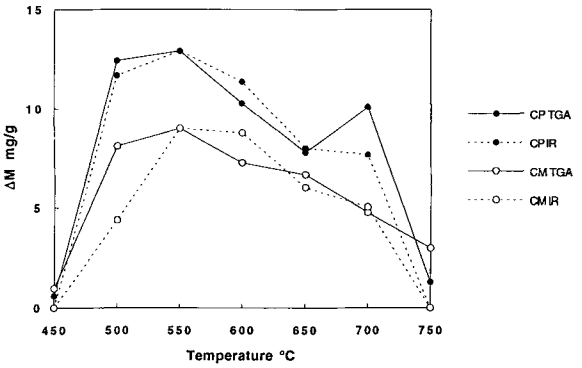

Figure 11. Plot of water content estimated by thermal analysis (TGA) and infrared transmission spectroscopy (IR) versus heating temperature for chlorites P (CP) and M (CM).

water and the 1610 cm^{-1} band to water bound to octahedral Mg at the edge of the structure. Both the zeolitic and bound water escape as the temperature increases. However, in the case of calcined chlorite, TGA experiments did not exhibit any discrimination between these two types of water. Then, bound water could prevent zeolitic water diffusion and outgassing temperature should be high enough to eliminate bound molecules and to allow diffusion of zeolitic water.

Two hypotheses could be proposed regarding the origin of this water; structural water or atmospheric (non-structural) water vapour. Experimental observations seem to favour the second hypothesis: 1) this water is released at temperatures lower than the dehydroxylation temperature of the interlayer sheet and 2) it is still present in samples which were calcined at temperature above the dehydroxylation temperature, i.e., 700°C. The atmospheric origin was confirmed by mass spectrometric analyses (Table 5) which reveal the presence of other condensed atmospheric gases such as Ar, N_2 and CO_2, released at the same temperature as trapped water. Furthermore, the quantities obtained by mass spectrometric analyses are coherent with the weight loss measured by TGA. Thus, atmospheric water vapour adsorbs in the solid during cooling of the samples.

Such an adsorption is possible only if very small pores exist in the solid. Argon adsorption isotherms confirm the presence of such pores. Indeed, when the sample is outgassed at high temperature, the shape of the isotherm (Figure 9) is typical of microporous solids (Type I in the classification of Brunauer *et al* 1940). If the same solid is outgassed at low temperature, water is still present in the micropores which are then not accessible to argon molecules (Figure 9). In this case, argon adsorbs only on the external surfaces of the solid. In the case of the microporous solid, the contribution of external surfaces can be subtracted from the total adsorbed amount. It yields the quantity of gaseous ar-

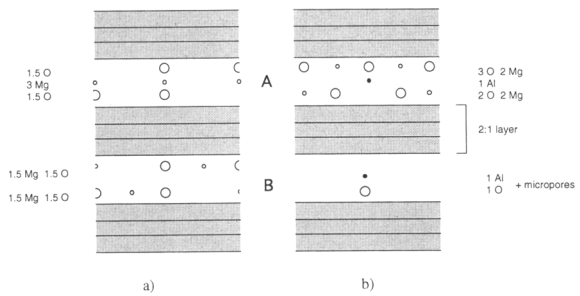

Figure 12. Schematic sketch of the possible structures obtained by dehydroxylation of the brucitic layer of Mg-chlorites. a: According to Brindley's model. b: According to a heterogeneous dehydroxylation model. Large open circles: O, small open circles: Mg, small filled circles: Al.

gon adsorbed in micropores which can then be converted into a liquid volume using the value of 1.427 (Anonymous 1976) for the specific density of liquid argon. This calculation leads to a value of 7.2×10^{-3} $cm^3 \cdot g^{-1}$, i.e., 7.2 mg/g of water. This value is very close to the weight loss obtained by TGA (7.3 mg/g).

The dehydroxylation mechanism proposed by Brindley and Chang (1974) can not explain the development of microporosity during brucitic dehydroxylation as the two resulting oxide sheets are filled by Mg and O atoms (Figure 12a). The model of Brindley and Chang involves migrations of atom over small distances so it can be designated as a homogeneous dehydroxylation mechanism. In some minerals, such as brucite and talc, a heterogeneous dehydroxylation is a more suitable mechanism to explain thermal transformations (Ball and Taylor 1961). In the heterogeneous dehydroxylation mechanism, a large scale migration of atoms occurs within the solid which is divided into acceptor and donor regions. The acceptor regions give protons, which migrate towards donor regions, and gain cations coming from donor regions. In the acceptor regions, the oxygen framework is not modified. In the donor regions, hydroxyls combine with protons, to form water molecules, which diffuse towards the surface and are removed from the solid. In this mechanism the donor regions are transformed into micropores. Kim *et al* (1987), Naono (1989) and Riebeiro-Carrott *et al* (1991) have observed such micropores after thermal decomposition of magnesium hydroxide. They showed the presence of two different types of micropores: 1) open micropores and 2) closed micropores not accessible to nitrogen.

Using this heterogeneous dehydroxylation model, it is now possible to explain the different phenomena involved in the interlayer dehydroxylation of clinochlores. The different steps involved in this mechanism can be presented as follows:

Donor region	Acceptor region
Initial state	
$Mg_2Al(OH)_6$	$Mg_2Al(OH)_6$

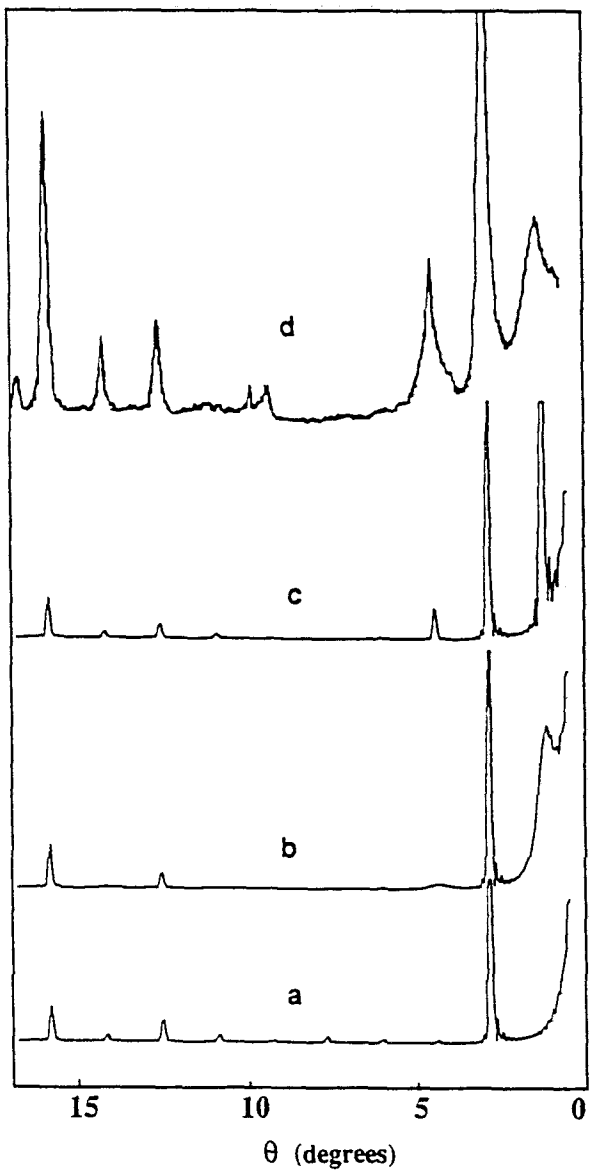

Figure 13. Comparison between experimental and simulated X-ray diffractograms of dehydroxylated Mg-chlorites. a: Simulated pattern obtained according to Brindley's model ($pAB = 1$). b: Simulated pattern obtained according to a heterogeneous dehydroxylation model ($pAB = 0.8$). c: Simulated pattern obtained according to a heterogeneous dehydroxylation model ($pAB = 1$). d: Experimental pattern.

At 550°C

$$(\square^{2-})_2Al(OH)_6 \underset{2\,Mg^{2+}}{\overset{4\,H^+}{\rightleftharpoons}} Mg_2Al(OH)_2(O^-)_4$$

Final state

$$AlO + (5\,H_2O)\uparrow \qquad Mg_4AlO_5 + (H_2O)\uparrow$$

We assume that only Mg cations are displaced whereas Al cations remain at their original position and balance the negative electrostatic charge defect due

to tetrahedral substitutions in the 2:1 layer. After thermal reaction, the dehydroxylated interlayer sheet is divided into areas enriched in MgO (acceptor regions) and porous areas with a deficit in MgO (donor regions) (Figure 12b). Micropores are then formed in these donor regions. When the sample cools, water adsorbs in these micropores where it can interact strongly with magnesium atoms located at the acceptor-donor frontier as evidenced by the IR band at 1610 cm^{-1}. Along the z-axis, interlayer donor and acceptor regions alternate in an irregular way. This leads to the broad long spacings reflections at 26–27 Å observed in the X-ray diffraction patterns of dehydroxylated chlorites. Further evidence can be obtained by simulating, along the z-axis, the X-ray patterns of the interstratified dehydroxylated structure. The simulation was carried out on the two structures presented in Figure 12 using the method proposed by Plançon and Tchoubar (1976). The results are shown in Figure 13.

The simulation according to Brindley-Chang model (Figure 13a) does not fit the experimental pattern. Indeed, it does not exhibit any peak around 27 Å, even in the case displayed in Figure 13a corresponding to regular interstratification. Furthermore, many 001 reflections are present on the simulated spectrum and absent on the experimental one. The fact that the results of Brindley and Chang could not be reproduced is very surprising. A simulated pattern calculated using a regular structure based on the 28 Å unit does not exhibit any 27 Å reflection. At the moment, this misfit is not explained.

The simulation according to the heterogeneous dehydroxylation mechanism was carried out in two cases; the first assuming a regular interstratification (Figure 13c). In this case, the simulated pattern exhibits a very intense peak around 27 Å which is more intense than the peak at 14 Å. The second assumed $pAB = pBA = 0.8$, where pij represents the probability of a layer of type j following a layer of type i in the stacking. In this case (Figure 13b), the simulated pattern exhibits nearly all the features of the experimental diffractogram (Figure 13d).

These results validate the heterogeneous dehydroxylation model. Furthermore, they suggest a tendency towards an ordered structure. Thus, it seems, as stated by Brindley and Chang (1974), that the process of dehydroxylation of one brucitic layer influences the process in adjacent interlayers.

CONCLUSIONS

Thermal transformations of Mg-chlorites, in the range of hydroxide octahedral layer dehydroxylation, probably lead to the formation of a heterogeneous structure with a 26–27 Å spacing. This structure can be described using a heterogeneous dehydroxylation mechanism. According to this model, the dehydroxylated interlayer octahedral sheet is divided into areas enriched in MgO (acceptor regions) and microporous regions (donor regions). The pores are filled by water when the mineral cools. Some water molecules interact strongly with the MgO walls located at donor-acceptor frontiers. High temperature conditions are needed to empty the micropores.

Modifications of the tetrahedral sheet are also observed after dehydroxylation. Experiments including HRTEM observations and low pressure gas adsorption are currently in progress to further characterize the structural transformations of clinochlore between 500 and 750°C.

ACKNOWLEDGMENTS

This research was supported by the European Economic Community: Program Raw Materials, grant Ma 2M CT90 0036 DTEE and the French "Ministère de la Recherche et de la Technologie," Program PHYGIS.

REFERENCES

Anonymous. 1976. *Gas Encyclopedia, L'Air Liquide.* Amsterdam: Elsevier, 1150 pp.

Bachiorrini, A., and M. Murat. 1986. Spectroscopie d'absorption infrarouge appliqué à la caractérisation de l'état d'amorphisation de la métakaolinite, Comptes Rendus de l'Académie des Sciences, Paris, Série II. **303**: 1783–1786.

Bai, T.-B., S. Guggenheim, S. J. Wang, D. G. Rancourt, and A. F. Koster Van Groos. 1993. Metastable phase relations in the chlorite H_2O system. *Amer. Mineral.* **78**: 1208–1216.

Ball, M. C., and H. F. W. Taylor. 1961. The dehydration of brucite. *Mineral. Mag.* **32**: 754–766.

Brindley, G. W., and S. Z. Ali. 1950. X-ray study of thermal transformations in some magnesian chlorites minerals. *Acta Crystalog.* **3**: 25–30.

Brindley, G. W., and T.-S. Chang. 1974. Development of long basal spacing in chlorites by thermal treatment. *Amer. Mineral.* **59**: 152–158.

Brindley, G. W., and J. Lemaitre. 1987. Thermal, oxydation and reduction reactions of clay minerals. In *Chemistry of Clays and Clay Minerals.* A. C. D. Newman, ed. London: Mineralogical Society, 319–370.

Brunauer, L. S., L. S. Deming, W. E. Deming, and E. Teller. 1940. On the theory of the Van der Waals adsorption of gases. *J. Amer. Chem. Soc.* **62**: 1723–1732.

Caillère, S., and S. Hénin. 1960. Influence des cations structuraux sur la température de déshydroxylation de certains minéraux phylliteux. *Bulletin de la Société Française de Céramique* **48**: 63–67.

Delmastro, A., A. Bachiorrini, and M. Murat. 1989. Désordre à courte distance dans les phases transitoires resultant de l'activation thermique des montmorillonites. *Clay Miner.* **24**: 43–52.

De Parseval, P. 1992. Etude minéralogique et géochimique du gisement de talc et chlorite de Trimouns. Doctorat de l'Université Paul Sabatier, Toulouse, 214 pp.

Emmet, P. H., and J. Brunauer. 1937. The use of low température van der Waals adsorption isotherms in determining the surface area by ion synthetic ammonia catalyst. *J. Amer. Chem. Soc.* **59**: 1553–1564.

Escoubes, M., and M. Karchoub. 1977. Contribution à l'étude du comportement des ions fer au cours de la déshydroxylation des minéraux argileux. *Bulletin de la Société Française de Céramique* **114**: 43–55.

Farmer, V. C. 1974a. In *The Infrared Spectra of Minerals.* London: Mineralogical Society, 87–110.

Farmer, V. C. 1974b. In *The Infrared Spectra of Minerals.* London: Mineralogical Society, 357.

Farmer, V. C. 1974c. In *The Infrared Spectra of Minerals.* London: Mineralogical Society, 344–347.

Griffiths, P. R., and J. S. Haseth. 1986. In *Fourier Transform Infrared Spectroscopy.* New York: Wiley-Interscience, 544.

Hayashi, H., R. Otsuka, and N. Imai. 1969. Infrared study of sepiolite and palygorskite on heating. *Amer. Mineral.* **53**: 1613–1624.

Heller, L., V. C. Farmer, R. C. Mackenzie, B. D. Mitchell, and H. F. W. Taylor. 1962. The dehydroxylation and rehydroxylation of trimorphic dioctahedral clay minerals. *Clay Miner.* **28**: 56–72.

Kim, M. G., U. Dahmen, and A. W. Searcy. 1987. Structural transformations in the decomposition of $Mg(OH)_2$ and $MgCO_3$. *J. Amer. Ceramic Soc.* **70**: 146–154.

McClellan, A. L., and H. F. Harnsberger. 1967. Cross sectional areas of molecules adsorbed on solid surfaces. *J. Colloid Interface Sci.* **23**: 577–599.

Michot, L., M. François, and J. M. Cases. 1990. Surface heterogeneity studied by a quasiequilibrium gas adsorption procedure. *Langmuir* **6**: 677–681.

Naono, H. 1989. Micropore formation due to thermal decomposition of magnesium hydroxyde. *Colloids and Surfaces* **37**: 55–70.

Plançon, A., and C. Tchoubar. 1976. Etude des fautes d'empilement dans les kaolinites partiellement désordonnées. II. Modèles d'empilement comportant des fautes de rotation. *J. Appl. Crystallog.* **9**: 279–285.

Riebeiro Carrott, M. M. L., P. J. M. Carrott, M. M. Brotas de Carvalho, and K. S. W. Sing. 1991. Microstructure of ex-hydroxyde magnesium oxyde and products of rehydration. In *Characterization of Porous Solids II.* F. Rodriguez-Reinoso, J. Rouquerol, K. S. W. Sing, and K. K. Unger, eds. Amsterdam: Elsevier, 635–643.

Sabatier, G. 1950. Sur l'influence de la dimension des cristaux de chlorites sur leurs courbes d'analyse thermique différentielle. *Bulletin de la Société Française de Minéralogie et de Cristallographie* **73**: 43–48.

Shirozu, H. 1980. Cation distribution, sheet thickness, and O-OH space in trioctahedral chlorites—An X-ray and infrared study. *Mineral. J.* **10**: 14–34.

Shirozu, H. 1985. Infrared spectra of trioctahedral chlorites in relation to chemical composition. *Clay Sci.* **6**: 167–176.

Shirozu, H., and K. Ishida. 1982. Infrared study of some 7 Å and 14 Å layer silicates by deuteration. *Mineral. J.* **11**: 161–171.

Villiéras, F. 1993. Etude des modifications des propriétés du talc et de la chlorite par traitement thermique. Doctorat de l'Institut National Polytechnique de Lorraine, Nancy, 568 pp.

Weiss, E. J., and R. A. Rowland. 1956. Oscillating-heating X-ray diffractometer studies of clay mineral dehydroxylation. *Amer. Miner.* **41**: 117–126.

Zimmermann, J.-L., A. Jambon, and G. Guyetand. 1988. Manometric and mass spectrometric analysis of fluids in geological materials. *Geochem. J.* **22**: 9–21.

(Received 5 January 1994; accepted 2 June 1994; Ms. 2451)